ACS APPLIED MATERIALS & INTERFACES

Research Article

www.acsami.org

Constructing High-Efficiency D−A−π−A-Featured Solar Cell Sensitizers: a Promising Building Block of 2,3-Diphenylquinoxaline for Antiaggregation and Photostability

Kai Pei,[†] Yongzhen Wu,[†] Ashraful Islam,[‡] Qiong Zhang,[†] Liyuan Han,*[,‡] He Tian,[†] and Weihong Zhu*[,†]

[†]Shanghai Key Laboratory of Functional Materials Chemistry, Key Laboratory for Advanced Materials and Institute of Fine Chemicals, East China University of Science and Technology, Shanghai 200237, People's Republic of China

[‡]Photovoltaic Materials Unit, National Institute for Materials Science, Sengen 1-2-1, Tsukuba, Ibaraki, Japan

Supporting Information

ABSTRACT: Controlling the sensitizer morphology on a nanocrystalline TiO_2 surface is beneficial to facilitating electron injection and suppressing charge recombination. Given that the grafted alkyl chain on a π-bridge thiophene segment for preventing π aggregation can deteriorate its intrinsic photostability, we incorporate a promising building block of 2,3-diphenylquinoxaline as the additional acceptor to construct a novel D−A−π−A-featured dye **IQ$_4$**, which exhibits several characteristics: (i) efficiently decreasing the molecular HOMO−LUMO energy gap by extending its absorption bands; (ii) showing a moderate electron-withdrawing capability for an ideal balance in both promising photocurrent and photovoltage; (iii) endowing an ideal morphology control with strong capability of restraining the intermolecular aggregation and facilitating the formation of a compact sensitizer layer via two twisted phenyl groups grafted onto the quinoxaline unit. The coadsorbent-free dye-sensitized solar cell (DSSC) based on dye **IQ$_4$** exhibits very promising conversion efficiency as high as 9.24 ± 0.05%, with a short-circuit current density (J_{sc}) of 17.55 mA cm^{-2}, an open-circuit voltage (V_{oc}) of 0.74 V, and a fill factor (FF) of 0.71 under AM 1.5 illumination (100 mW cm^{-2}). **IQ$_4$**-based DSSC devices with an ionic liquid electrolyte can keep constant performance during a 1000 h aging test under 1 sun at 60 °C. Because of spatial restriction, the two phenyl groups grafted onto the additional electron-withdrawing quinoxaline are demonstrated as efficient building blocks, not only improving its photostability and thermal stability but also allowing it to be a successful antiaggregation functional unit. As a consequence, the incorporated 2,3-diphenylquinoxaline unit can realize a facile structural modification for constructing organic coadsorbent-free D−A−π−A-featured sensitizers, thus paving a way to replace the common, stability-deleterious grafted alkyl chain on the thienyl bridge.

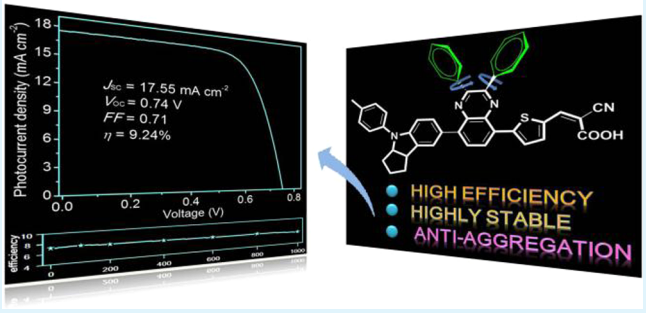

KEYWORDS: *solar cells, organic sensitizers, quinoxaline, antiaggregation, photostability*

INTRODUCTION

Dye-sensitized solar cells (DSSCs) are under intensive interdisciplinary investigation in both academia and industry worldwide because of the cost-effective and flexible solar energy conversion.[1−8] As the key component of DSSCs, the pure metal-free organic sensitizers with the common donor−π-bridge−acceptor (D−π−A) configuration are strongly desirable because of their several features, such as large absorption coefficients, feasible molecular tailoring with optoelectronic properties, cost-effective facile preparation processes, and no concern on the limited ruthenium (Ru) resource.[9−12] However, the power conversion efficiencies (η) of DSSCs are generally lower than those based on Ru complexes. To date, there are only a few pure metal-free organic sensitizers based on an iodine electrolyte that are capable of achieving 9% in photovoltatic efficiency.[13−17] Yet, the concern on the critical device stability is still under great challenge. The major reason for the low performance of DSSCs based on metal-free sensitizers is the relatively low open-circuit photovoltage (V_{oc}), possibly resulting from a shorter electron lifetime with respect to Ru counterparts.[18−20] Special attention is focused on the energy losses, especially for dye regeneration,[21−23] a vital factor to shrink V_{oc} values.[24,25]

Controlling the assembly morphology of sensitizers on the nanocrystalline TiO_2 surface is expected to facilitate electron injection and suppress charge recombination. Although some aggregates would be useful to form a compact dye layer on the TiO_2 surface and avoid the electrolyte-contacting injected electrons, the electron injection efficiency is always influenced by the quenching of excited states (such as intermolecular

Received: February 28, 2013
Accepted: May 20, 2013
Published: May 20, 2013

   dx.doi.org/10.1021/am400754d | ACS Appl. Mater. Interfaces 2013, 5, 4986−4995

energy and/or electron transfer) because of the strong intermolecular interaction within the compact dye layer.[26−29] Thus, it is critical to keep a balance in the compact dye layer with controlled intermolecular aggregation. Generally, there are two strategies to solve the self-aggregation problem of metal-free organic sensitizers. Co-adsorption with steric hindrance species,[30] such as deoxycholic acid derivatives (DCA and CDCA), is usually applied to block dye aggregation whereas it reduces the dye coverage ratio on TiO_2 surface and requires critical optimization with adsorption conditions (for instances, solvents, dyes and coadsorbent concentrations). For increasing the self-antiaggregation tendency in D−π−A sensitizers, another efficient method is to specifically incorporate steric hindered alkyl chains onto π-bridge,[31−34] donor[35−37] and acceptor moieties.[16] We have found that the introduction of a long alkyl chain into the donor part has little effect on preventing molecular aggregation because of the good coplanarity of the π linker, suggesting that the most effective way to prevent π aggregation is still the incorporation of long alkyl groups into a π-bridge segment.[35] However, the incorporation of an alkyl chain on a thiophene bridge can decrease its intrinsic photostability to some extent.[15,38,39] Accordingly, to further boost the efficiency of DSSCs with long-term stability, further insight into the π linker in D−π−A organic sensitizers should be conducted, especially for finding an alternative to the common incorporation of an alkyl chain on the thiophene bridge.

Recently, D−A−π−A-featured sensitizers in which an additional electron-withdrawing unit is successfully incorporated into the π bridge for tailoring molecular structures, optimizing energy levels, and improving the photostability to a great extent have become attractive.[40−51] Geng et al. theoretically verify the DSSC performance sensitized by D−A−π−A dyes with a more suitable structure compared to D−π−A and D−π−A−A architectures.[52] The broad spectral response with high photocurrent is facilely achieved in benzothiadiazole-based D−A−π−A sensitizers, while their V_{oc} value is always limited to 700 mV;[48,49] in contrast, high V_{oc} is easy to realize in benzotriazole-based D−A−π−A sensitizers, but their photocurrent becomes disappointed to some extent.[50,51] It would become desirable to possess both high J_{sc} of benzothiadiazole dyes and high V_{oc} of benzotriazole dyes simultaneously. Given that the electron-withdrawing ability of benzothiadiazole is somewhat too strong while that of benzotriazole is a little weak, the moderate quinoxaline unit might be an ideal electron-withdrawing unit for constructing efficient D−A−π−A-featured sensitizers,[53−57] especially expecting to realize a balance in both promising photocurrent and photovoltage. With these in mind, we incorporate an electron-withdrawing unit of 2,3-diphenylquinoxaline as the additional acceptor to construct a novel D−A−π−A-featured dye **IQ$_4$** (Figure 1) for efficiently decreasing the molecular highest occupied molecular orbital (HOMO)−lowest unoccupied molecular orbital (LUMO) energy gap and tailoring their absorption spectra. Moreover, two twisted phenyl groups grafted onto the quinoxaline unit are demonstrated to endow a strong capability of restraining intermolecular aggregation with ideal morphology. That is, the incorporated additional acceptor unit of 2,3-diphenylquinoxaline in a D−A−π−A configuration can realize a facile structural modification for achieving high self-antiaggregation, instead of the traditionally grafting long alkyl on the thiophene bridge. To further verify the antiaggregation ability of the 2,3-diphenylquinoxaline unit, a

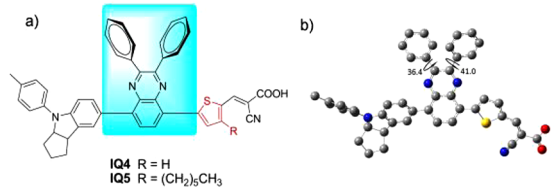

Figure 1. (a) Chemical structures of sensitizers **IQ$_4$** and **IQ$_5$**. (b) Optimized ground-state geometry of **IQ$_4$** calculated at the hybrid density functional theory (B3LYP) with a 6-31G* basis set as implemented in the *Gaussian 09* program.

reference dye **IQ$_5$** is also designed with a hexyl chain on the thienyl unit. Impressively, using a liquid electrolyte, the coadsorbent-free DSSC based on dye **IQ$_4$** exhibits a very promising conversion efficiency (η) of 9.24 ± 0.05% with a short-circuit current density (J_{sc}) of 17.55 mA cm^{-2}, an open-circuit voltage (V_{oc}) of 0.74 V, and a fill factor (FF) of 0.71 under AM 1.5 illumination (100 mW cm^{-2}), which is superior to the performance of **IQ$_5$** (η = 8.65 ± 0.05%, J_{sc} = 16.03 mA cm^{-2}, V_{oc} = 0.75 V, and FF = 0.72) under the same conditions. In contrast, coadsorption with 20 mM DCA in a dye bath of **IQ$_4$** decreases its photovoltaic performance by a decrease of the photocurrent (J_{sc} = 16.16 mA cm^{-2}, V_{oc} = 0.74 V, FF = 0.68, and η = 8.18 ± 0.05%). Moreover, the stability of the quinoxaline sensitizers, which was not given much attention in other similar researches.[53,55,57] is also carefully tested. In this paper, **IQ$_4$**-based DSSC devices with an ionic liquid electrolyte are fabricated and show high efficiency (7.34%), keeping a constant performance during a 1000 h aging test under 1 sun at 60 °C. Overall, the incorporation of additional 2,3-diphenylquinoxaline in a D−A−π−A configuration can not only allow it to be a successful antiaggregation functional unit but also improve its photostability and thermal stability. Because of steric restriction, the two phenyl groups grafted onto the additional electron-withdrawing quinoxaline are efficient building blocks for achieving high V_{oc} by preventing aggregation and reducing charge recombination, thus paving a way to replace the common, stability-deleterious alkyl-substituted thienyl bridge to develop high efficiency coadsorbent-free organic sensitizers.

RESULTS AND DISCUSSION

Design and Synthesis. As shown in Figure 1, for the design of sensitizers **IQ$_4$** and **IQ$_5$**, we employed the strong electron-donating unit of indoline as the electron donor[58−60] and frequently used cyanoacetic acid as the acceptor/anchor and a thiophene moiety as the conjugated bridge. Additionally, an electron-withdrawing quinoxaline unit was incorporated between the donor and π-conjugation unit. Previously, we have demonstrated that the additional acceptor unit in the π bridge can effectively decrease the molecular HOMO−LUMO energy gap, red-shift electronic absorption spectra, and facilitate intramolecular electron migration from the donor to the cyanoacetic acetic unit. Moreover, synthetic processes indicate that the electron-deficient quinoxaline unit can distinctly improve the photostability of indoline-based organic sensitizers. As shown in Figure 2, the bare indoline is extremely photosensitive and deteriorated in a short time. After connected with the quinoxaline unit, the intermediate becomes very stable. The increase in the photostability of indoline derivatives can be attributed to the decreased molecular LUMO energy level with a beneficial electron distribution between electron-donating indoline and electron-withdrawing quinoxa-

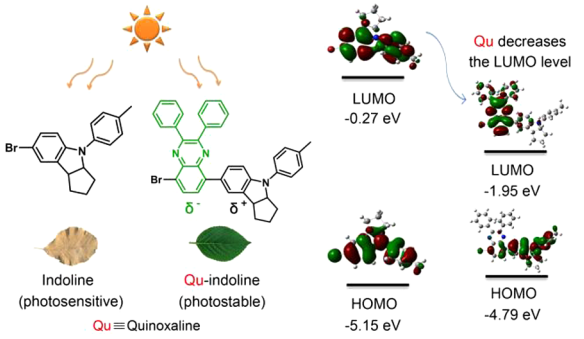

Figure 2. Quinoxaline unit increasing the photostability of indoline derivatives.

line units (Figure 2). Such superiority in improving the photostability of indoline-containing derivatives is beneficial to not only the synthetic process but also the stability of DSSCs. As is well-known, the intermolecular $\pi-\pi$ stacking and unfavorable aggregation, which may lead to a drastic decrease in the photovoltaic performance, are ubiquitous in organic sensitizers. To reduce the intermolecular $\pi-\pi$ interaction, a couple of phenyl groups were grafted on the quinoxaline unit for restraining aggregation by their twisted spatial arrangement. A reference dye **IQ$_5$** with a hexyl chain on the thienyl bridge unit was also synthesized to systematically examine the antiaggregation ability of the diphenylquinoxaline unit as well as the photostability.

Absorption Properties. The UV−visible absorption spectra of **IQ$_4$** and **IQ$_5$** in a dilute CH_2Cl_2 solution are depicted in Figure 3a. Their absorption curves are almost identical because of the similar chemical structure of the conjugated backbone. Owing to the introduction of an electron-withdrawing quinoxaline unit into a strong electron-donating indoline unit, both dyes show a broad absorption range covering a large proportion of the visible region, thus ensuring fertile light harvesting. As a typical D−A−π−A configuration, both dyes exhibit three absorption bands around the 330, 425, and 530 nm regions (Figure 3a). The band positions (λ_{max}) and corresponding molar absorption coefficients (ε) of the absorption peaks are listed in Table 1. A distinct charge-transfer (CT) absorption band (band 1) is observed at around 530 nm for both dyes. How the absorbed photons populate in the absorption bands will be investigated in the following discussion by employing theoretical calculation.

When carboxylic acid (−COOH)-based sensitizers are anchored onto a nanocrystalline TiO_2 surface, deprotonation[61] of the −COOH group as well as intermolecular aggregation severely affects the absorption behaviors. Generally, deprotonation and *H*-aggregation (a type of dye with an absorption band that shifts to a longer wavelength of increasing sharpness when it aggregates under the influence of a solvent or additive or concentration as a result of supramolecular self-organization) usually result in a blue shift in the CT band, while *J*-aggregation (a one-dimensional array of molecules in which the transition moments of individual monomers are aligned parallel to each other but perpendicular to the line joining their centers) mainly leads to a red shift. In addition, the thicknesses of the TiO_2 films also influences the shapes of the absorption curves. As shown in Figure 3b, upon adsorption on the relatively thin TiO_2 films (4 μm), absorption bands can be distinguished for both dyes, and their CT bands shift to short wavelength by

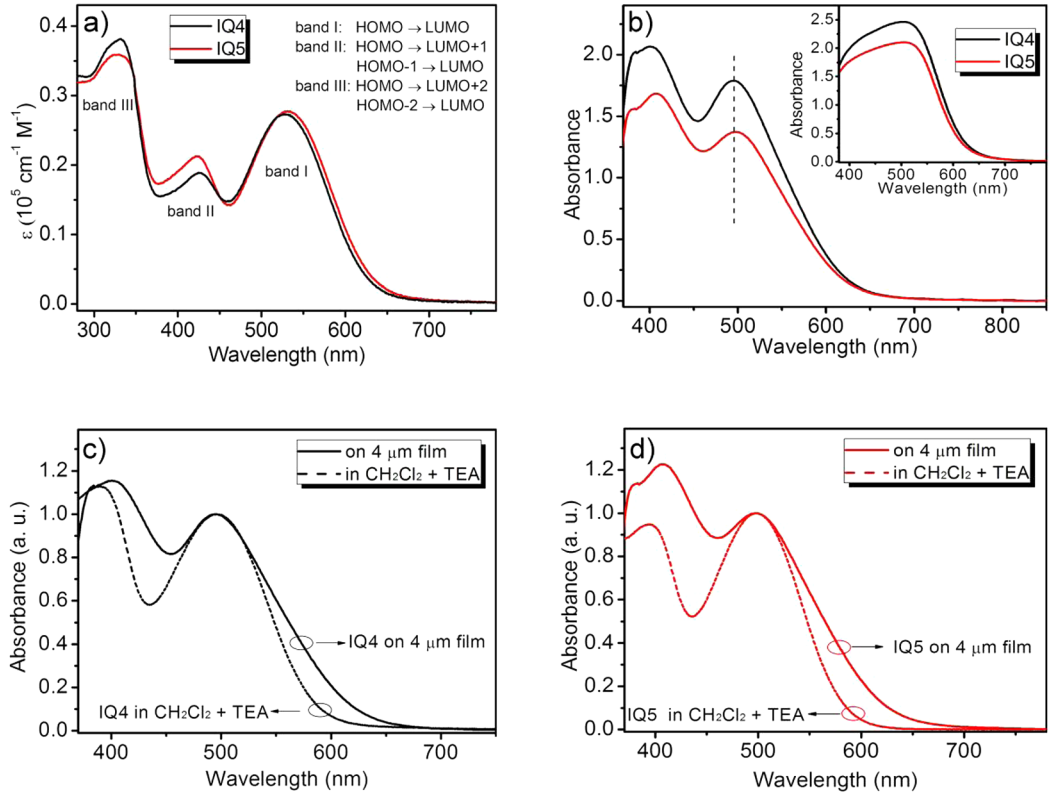

Figure 3. Absorption spectra of **IQ$_4$** and **IQ$_5$** (a) in CH_2Cl_2 and (b) on 4 μm TiO_2 thin films. Inset: 8 μm TiO_2 thick film. Normalized absorption spectra of (c) **IQ$_4$** and (d) **IQ$_5$** in a CH_2Cl_2 solution and on 4 μm TiO_2 films.

Table 1. Photophysical and Electrochemical Data of IQ_4 and IQ_5

dye	$\lambda_{max}{}^a$/nm	ε^a/M^{-1} cm^{-1}	HOMO^b/V	$E_{0-0}{}^{cvc}$/V	LUMO^{cvc}/V	$E_{0-0}{}^{opt d}$/V	LUMO$^{opt d}$/V
IQ_4	529	27300	0.67	2.09	−1.42	1.95	−1.28
	425	18900					
	334	38000					
IQ_5	531	27700	0.66	2.07	−1.47	1.93	−1.27
	425	21200					
	325	35900					

[a]Absorption peaks (λ_{max}) and molar extinction coefficients (ε) were measured in CH_2Cl_2. [b]The formal oxidation potentials (vs NHE) in CH_2Cl_2 were calibrated with ferrocene and taken as the HOMO. [c]Calculated from CV curves. [d]Estimated from the band gap derived from the wavelength at 10% maximum absorption intensity for the dye in CH_2Cl_2.

approximately 30 nm. On thicker films (8 μm), the absorption thresholds of both two dyes become broader. Meanwhile, their two distinguishable absorption bands develop as a single absorption plateau (inset in Figure 3b). Moreover, although the ε values of both dyes are almost the same in solution, the absorbance of a IQ_4-loaded TiO_2 film is always higher than that of IQ_5, suggesting that the long alkyl chain on the π-thienyl bridge in the system of IQ_5 can result in the lower adsorption amount in the unit volume of porous TiO_2. In order to identify the fact that CT bands blue-shift by 30 nm from a dye solution to sensitized 4 μm TiO_2 films, a set of deprotonation experiments were conducted on both dyes in CH_2Cl_2 solutions by the addition of an excess amount of triethylamine (TEA). As shown in Figure 3c,d, the peak wavelength of the CT absorption band induced by the effect of TEA is quite similar to that of chemical adsorption onto 4 μm TiO_2 films. That is, the blue shift in the CT absorption band during the adsorption process should be predominated by the deprotonation effect of the −COOH group rather than intermolecular aggregation. Accordingly, the two phenyl groups on the quinoxaline unit seem to account for the antiaggregation function in both dyes. Actually, the optimized configuration of IQ_4 (Figure 1b) indicates that the two phenyl groups are spatially twisted to a large nonplanar degree to quinoxaline (36.4 and 41.0°), which may effectively restrain intermolecular $\pi-\pi$ stacking.[62]

Energy Levels and Orbital Distributions. Energy levels of sensitizers such as HOMO and LUMO are crucial to electron injection and dye regeneration in DSSC operations. Cyclic voltammetries (CVs) were employed on IQ_4 and IQ_5 in CH_2Cl_2 to roughly estimate their energy levels (Figure 4a). The HOMO and LUMO energies determined from the first oxidation and reduction potentials are +0.67 and −1.42 V vs NHE for dye IQ_4 and + 0.66 and −1.47 V for IQ_5 (Table 1), respectively. Dyes IQ_4 and IQ_5 show energy gaps ($E_{0-0}{}^{CV}$) of 2.09 and 2.07 eV, respectively, which are in good accordance with the band gaps determined from the optical studies ($E_{0-0}{}^{opt}$). The HOMO values are more positive than commonly used I^-/I_3^- redox couples (~0.4 V vs NHE), and LUMO energy levels lie above the conduction band edge of TiO_2 (~−0.5 V vs NHE), thus ensuring a sufficient driving force for electron injection and dye regeneration.[63]

Photoinduced electron transition in sensitizers is a key process for photovoltaic conversion. Photons from different wavelengths can excite ground-state electrons to different excited states. Time-dependent density functional theory (TDDFT) is used to analyze the excitation pathways and understand the injection process under different portions of sunlight irradiation.[64,65] Taking IQ_4 as an example, the observed three bands in absorption spectra are caused by several kinds of electron excitation (Table 2). The low-energy

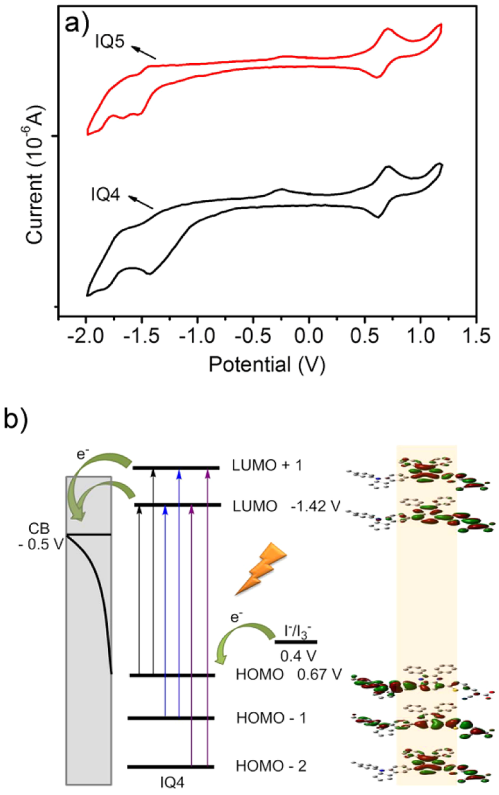

Figure 4. (a) CV curves of IQ_4 and IQ_5 in a CH_2Cl_2 solution vs NHE. (b) Schematic diagram of the energy band structure and major electron-transfer processes in DSSCs based on IQ_4.

Table 2. Calculated TDDFT Excitation Energies (E, eV and nm), Oscillator Strengths (f), and Composition in Terms of Molecular Orbital Contributions of IQ_4

dye	state	composition[a]	E (eV, nm)	f
IQ_4	S1	85% H → L	2.44 (507.2)	0.9815
	S2	50% H_{-1} → L	3.15 (393.3)	0.5636
		39% H → L_{+1}		
	S3	62% H_{-2} → L	3.60 (344.4)	0.1343
		73% H → L_{+2}	3.87 (320.7)	0.2212

[a]H = HOMO, L = LUMO, H_{-1} = $HOMO_{-1}$, H_{-2} = $HOMO_{-2}$, L_{+1} = $LUMO_{+1}$, L_{+2} = $LUMO_{+2}$.

band located at 529 nm (band I) is ascribed to HOMO → LUMO transition, the middle band at 425 nm (band II) is composed of HOMO → $LUMO_{+1}$ and $HOMO_{-1}$ → LUMO, and the UV band (band III) around 330 nm is due to some high-energy transitions, such as $HOMO_{-2}$ → LUMO and HOMO → $LUMO_{+2}$. Obviously, most transitions move excited

electrons to LUMO and $LUMO_{+1}$ orbitals; hence, checking the electron distribution of these two orbitals is pivotal for evaluating electron injection in view of orbital overlapping between sensitizer and TiO_2. Density functional theory (DFT) calculation on **IQ_4** indicates that the electrons of both LUMO and $LUMO_{+1}$ are delocalized over the A−π−A moiety with a large composition on the anchoring group, where the electron is close to the TiO_2 surface and can be smoothly injected into the conduction band of the TiO_2 semiconductor (Figure 4b). Therefore, photons from each of the three absorption bands are useful for electron injection and photovoltaic conversion. However, because the $LUMO_{+2}$ orbital is mainly located on the quinoxaline unit [Figure S1, Supporting Information (SI)], it is far from the anchoring group, thus contributing little to the electron injection with the transition from HOMO to $LUMO_{+2}$. Moreover, the distributions of most ground and excited frontier orbitals (such as $HOMO_{-2}$, $HOMO_{-1}$, HOMO, LUMO, and $LUMO_{+1}$ in Figure 4b) of **IQ_4** are well overlapped with the quinoxaline unit, indicating that the photoexcited electrons could be successively transferred from the donor to the quinoxaline unit, then transferred to the cyanoacetic acid subunit, and finally to TiO_2. It is consistent with our expected cascaded electron-trap role of the incorporated quinoxaline unit.[48]

Solar Cell Performances. Figure 5 shows the current−voltage (J−V) characteristics and incident photon-to-current conversion efficiency (IPCE) action spectra of liquid electrolyte-based DSSCs obtained with **IQ_4** and **IQ_5**. The effect of additives in electrolyte (4-*tert*-butylpyridine, TBP) and coadsorbent (DCA) on the photovoltaic performances is systematically studied. The IPCE spectra (Figure 5a) illustrate that the visible light can be converted to photocurrent efficiently in the range of 300−800 nm, which is in good accordance with the absorption spectra of sensitizers on the TiO_2 film. Especially, the DSSC based on **IQ_4** displayed IPCE higher than 80% in the plateau region of 380−610 nm with a maximum nearly reaching about 90%, whereas reference dye **IQ_5** showed a little narrower response. Such broader spectral responses of **IQ_4** and **IQ_5** provide good light-harvesting ability for long-wavelength visible light, which would be attributed to the concerted contribution from both the electron-withdrawing properties of the quinoxaline unit and the strong electron-donating abilities of the indoline group. Figure 5b shows the current−voltage (J−V) curves of **IQ_4** and **IQ_5**, and detailed parameters such as J_{sc}, V_{oc}, FF, and η, under different conditions, are listed in Table 3. Both dyes show considerably high power conversion efficiency (>8%) without any further optimization. Especially, **IQ_4**-based DSSCs without DCA coadsorption resulted in a very promising efficiency as high as 9.24% under standard measurement.

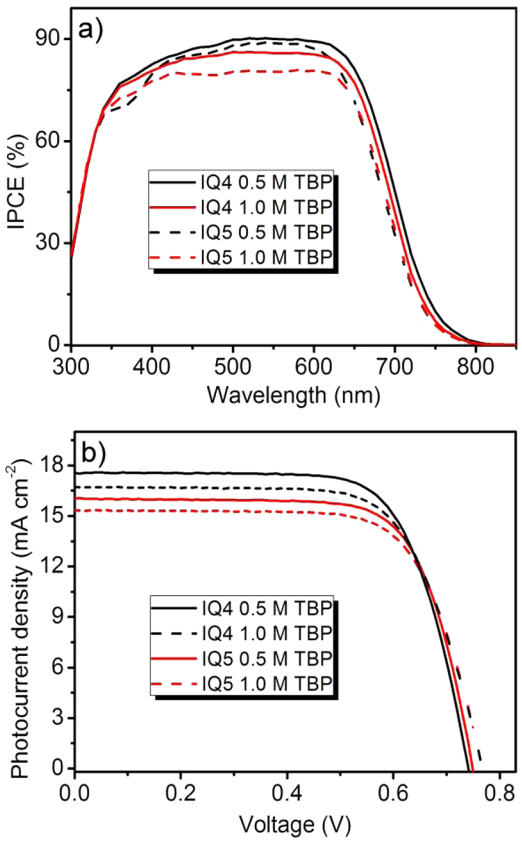

Figure 5. Photovoltaic performance of DSSCs sensitized with **IQ_4** and **IQ_5**: (a) IPCE action spectra; (b) photocurrent density vs voltage (J−V) curves with TBP (0.5 and 1.0 M) in electrolytes.

As is well-known, TBP is a commonly used species in electrolytes for the sake of improving V_{oc} and η because coordination between electronegative pyridine and TiO_2 could shift the TiO_2 conduction band edge toward higher energy level. Additionally, TBP can cover the defect of the dye monolayer to block the dark current and increase the electron lifetime.[66−68] **IQ_4**-based DSSCs gave V_{oc} of 0.74 V when the TBP concentration was 0.5 M. Increasing the TBP concentration to 1.0 M led to a gain of 30 mV in V_{oc} but a loss of 0.8 mA cm^{-2} in J_{sc}. This means that the LUMO orbital of **IQ_4** is sufficiently higher than the conduction band of TiO_2; electron injection becomes a little difficult when increasing the TBP content. Overall, the loss in J_{sc} is larger than the increase in V_{oc} by increasing the TBP concentration, resulting in lower η of 8.85 ± 0.05% than the initial 9.24 ± 0.05% (Figure 5b). A very similar phenomenon has been observed in **IQ_5**-based DSSCs (Table 3).

Sterically hindered DCA is often used as the coadsorbent in a dye bath for suppressing dye aggregation.[30] As discussed above, for **IQ_4** and **IQ_5**, the incorporated 2,3-diphenylquinoxaline unit is expected to restrain intermolecular π−π stacking when dyes are tightly assembled on the TiO_2 surface. The discussion on the absorption properties of **IQ_4**- and **IQ_5**-sensitized TiO_2 films has partly disclosed the antiaggregation function of both dyes. Here, the coadsorption strategy with DCA is further applied to examine the contribution of the 2,3-diphenylquinoxaline unit. As shown in Table 3, coadsorption with 20 mM DCA in a bath of **IQ_4** does not affect the V_{oc} performance (keep 0.74 V) but severely decreases the J_{sc} value (from 17.55 to 16.16 mA). Apparently, DCA is unnecessary for **IQ_4**-based DSSCs. It is not difficult to understand that **IQ_5**-based DSSCs do not need coadsorbent as well because of the presence of an additional alkyl chain. Moreover, with respect to **IQ_5**, the higher performance of DCA-free DSSCs based on **IQ_4** suggests that the alkyl chain in **IQ_5** is also needless. Presumably, the presence of an alkyl chain on the π-thienyl bridge increases the molecular bulk of **IQ_5**, thus decreasing the adsorption amount of the sensitizers in porous TiO_2 films. Obviously, the incorporated 2,3-diphenylquinoxaline unit is a successful alternative to traditional alkyl chains grafted onto the thiophene bridge. Moreover, the 2,3-diphenyl groups grafted onto the quinoxaline unit (dye **IQ_4**, η = 9.24 ± 0.05%) are prior to the long alkyloxy

Table 3. Photovoltaic Performances for IQ_4 and IQ_5-Based DSSCs

dye	TBP/M	DCA/mM	V_{OC}/V	J_{SC}/mA cm^{-2}	FF/%	η/%
IQ_4	0.5	0	0.74 ± 0.05	17.55 ± 0.4	71 ± 1	9.24 ± 0.05
	0.5	20	0.74 ± 0.05	16.16 ± 0.5	68 ± 1	8.18 ± 0.05
	1.0	0	0.77 ± 0.07	16.72 ± 0.5	69 ± 1	8.85 ± 0.05
IQ_5	0.5	0	0.75 ± 0.08	16.03 ± 0.3	72 ± 1	8.65 ± 0.05
	1.0	0	0.77 ± 0.08	15.33 ± 0.3	71 ± 1	8.33 ± 0.05

group couterpart (dye **IQ_2**, η = 8.50 ± 0.05%).[52] As a consequence, **IQ_4** obtains an excellent performance without coadsorbent; that is, the incorporated sterically hindered 2,3-diphenylquinoxaline unit can keep a morphology balance between antiaggregation and the compact sensitizer layer on the TiO_2 surface, realizing a beneficial electron injection with low charge recombination.[26−29]

Interestingly, the 2,3-diphenylquinoxaline-based D−A−π−A sensitizer **IQ_4** exhibits both high J_{sc} (>17 mA cm^{-2}) and promising V_{oc} (>700 mV). Among D−A−π−A configuration sensitizers, the merits of a reported additional acceptor of benzothiadiazole[48,49] (broad spectral response) and benzotriazole[50,51] (high photovoltage) units are simultaneously embodied in the specific quinoxaline structure. The preferable features for such high performance of **IQ_4** are attributed to its broad photoresponse and beneficial adsorption morphology on the TiO_2 surface. Overall, the mild electron-withdrawing and nonplanar character of 2,3-diphenylquinoxaline makes it a perfect building block for constructing high-efficiency D−A−π−A-featured organic sensitizers.

Electrochemical Impedance Spectroscopy (EIS). The high photocurrent of **IQ_4**-based DSSCs is not difficult to understand from its broad and high IPCE response. In contrast, the insight into its high V_{oc} (about 100 mV higher than the reported benzothiadiazole analogues[48,49]) is very worthy of investigation. Generally, for well-operational DSSCs, the V_{oc} performance is closely sensitive to the CT processes at the TiO_2/dye/electrolyte interface,[69−73] which can be elucidated by EIS.[74,75] Figure 6 compares EIS plots for **IQ_4**- and **IQ_5**-sensitized cells measured in the dark at a forward bias of −0.75 V. Furthermore, the equivalent circuit presented in Figure 6c was used to analyze the reaction resistance of the DSSCs, and corresponding parameters are listed in Table 4. In Nyquist plots, the small and large semicircles located in the high- and middle-frequency regions are assigned to CT at platinum/electrolyte and TiO_2/dye/electrolyte interface, respectively.[76−80] Another small semicircle at the low-frequency region is overlapped with the middle-frequency large semicircle. Generally, the incorporation of long alkyl chains into organic push−pull sensitizers is regarded as an efficient approach to improving the dye layer morphology on TiO_2 and restraining charge recombination, thus remarkably increasing the radius of the midsemicircle (in Nyquist plots) and moving the phase angle peak (in Bode plots) to low frequency.[32,51] Apparently, from Figure 6, the introduction of a hexyl chain on the thiophene π linker in **IQ_5** exhibits very similar EIS behavior with respect to that of **IQ_4** because the radius of the middle semicircle in Nyquist plots and the peak frequency in Bode plots for both dyes are almost comparable. As is known, the electron lifetime's reciprocal is associated with the charge recombination rate, which is related to the characteristic frequency of the lower frequency peak in the Bode plot. Thus, the electron lifetime (τ_n) can be estimated from $\tau_n = 1/(2\pi f_p)$, where f_p is the peak frequency in the lower frequency region.

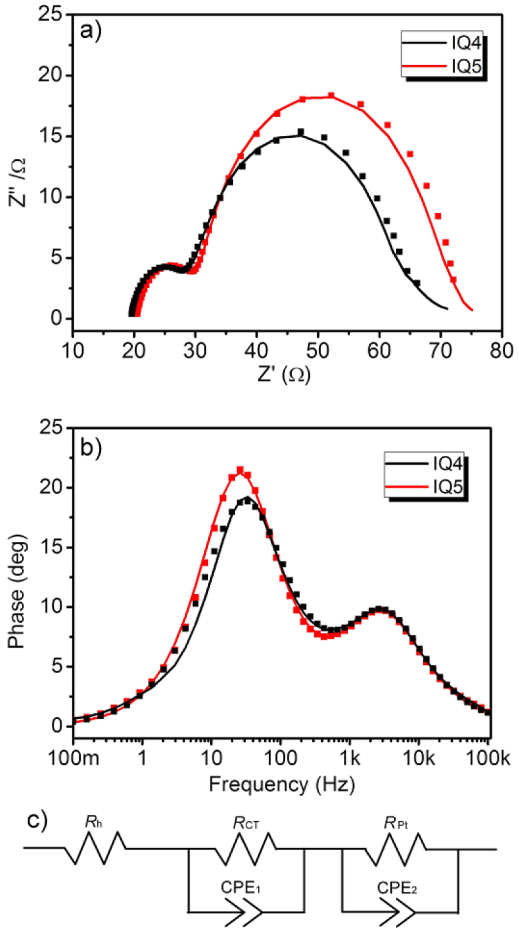

Figure 6. EIS Nyquist (a) and Bode (b) plots and equivalent circuit (c) for DSSCs based on **IQ_4** and **IQ_5** measured in the dark at a forward bias of −0.75 V. The lines of parts a and b show theoretical fits using the equivalent circuits (c).

IQ_4 and **IQ_5** shows similar τ_n values, 4.74 and 6.14 ms. The high photovoltaic performance of **IQ_4** and its almost same response with **IQ_5** in EIS measurement indicate that 2,3-diphenylquinoxaline is a successful building block in organic sensitizers for preferably controlling the adsorption morphology of sensitizers onto TiO_2. That is, EIS results provide evidence that, due to spatial restriction, the two phenyl groups grafted onto the additional electron-withdrawing quinoxaline can endow strong self-antiaggregation, competent in retarding unfavorable charge recombination.

Long-Term Stability of Dyes and Devices. Stability is a key factor for evaluating the practical application of DSSCs. Each component as well as sealing technique of cell devices can impact its stability to different extents during long-term application under severe environments. As the core of DSSCs, the sensitized dye should be stable enough under light irradiation as a precondition for a long-term stable device.

dx.doi.org/10.1021/am400754d | ACS Appl. Mater. Interfaces 2013, 5, 4986−4995

Table 4. Parameters Obtained by Fitting the Impedance Spectra of DSSCs Based on IQ_4 and IQ_5 via the Equivalent Circuit[a]

cell	IQ_4	IQ_5
$R_h/\Omega\ cm^{-2}$	19.53	20.42
$R_{CT}/\Omega\ cm^{-2}$	38.66	42.54
n_1	0.8414	0.9028
CPE1/Sn cm^{-2}	4.821×10^{-4}	3.768×10^{-4}
$R_{Pt}/\Omega\ cm^{-2}$	8.976	9.817
n_2	0.8652	0.8566
CPE2/Sn cm^{-2}	2.521×10^{-5}	2.655×10^{-5}
τ_n/ms	4.74	6.14

[a]Equivalent circuit of the DSSC consisting of TiO_2/dye/electrolyte and platinum/electrolyte interface (Figure 6c); R_h, R_{CT}, and R_{Pt} are the series resistance of platinum and FTO glass and the CT resistance at platinum/electrolyte and at TiO_2/dye/electrolyte interface, respectively; CPE1 and CPE2 are the constant-phase elements for the TiO_2/dye/electrolyte and platinum/electrolyte interface, respectively. n presents the degree of surface inhomogeneity; τ_n is calculated from the relationship $\tau_n = 1/(2\pi f_p)$.

Katoh and co-workers have developed a simple and efficient method to evaluate the photostability of dyes in a short period of time.[81] Because the most unstable state of sensitizers is in the regeneration process, the corresponding dyes must remain stable in the cation state for at least 10 s to be capable of realizing a 10-year operation cycle.[81] To shorten the experiment period, we can accelerate the dye aging process by light irradiation on a dye-loaded TiO_2 electrode. Without an electrolyte, dye regeneration could occur only by the receipt of injected electrons in TiO_2, which takes 10^4–10^3 times longer than that in complete solar cell device in time scale. Figure 7a illustrates the experimental method and dye regeneration mechanism. After 45 min of light irradiation on corresponding dye-sensitized TiO_2 electrodes, the absorbance of **IQ_4** maintained almost unchanged while that of **IQ_5** decreased to some extent (Figure 7c,d). Meanwhile, the color of the **IQ_4**-loaded TiO_2 film could remain purple throughout the whole experiment while the **IQ_5**-based film faded from purple to light red. Such a difference in responses to light irradiation between **IQ_4** and **IQ_5** reveals that the photostability of the former is significantly prior to the latter, indicating the detrimental effect of an alkyl chain on the thienyl bridge in **IQ_5**.[37] For further evaluation of the practical stability of **IQ_4**-based DSSC during the long term, a less volatile ionic liquid electrolyte (containing 0.6 M 1-propyl-3-methylimidazolium iodide, 0.15 M iodine, 0.1 M guanidiniumthiocyanate, and 0.5 M NMBI in 3-methoxypropionitrile) was employed. Hence, the photovoltaic performance of devices in this experiment was a little lower than the above-mentioned volatile electrolyte device. The resulting DSSCs based on **IQ_4** with an ionic liquid electrolyte offered J_{sc} = 14.0 mA, V_{oc} = 735 mV, and FF = 0.71, corresponding to η of 7.34%. Figure 7b shows variations of the photovoltaic parameters during a long-term accelerated aging on **IQ_4**-based solar cells, keeping a constant performance

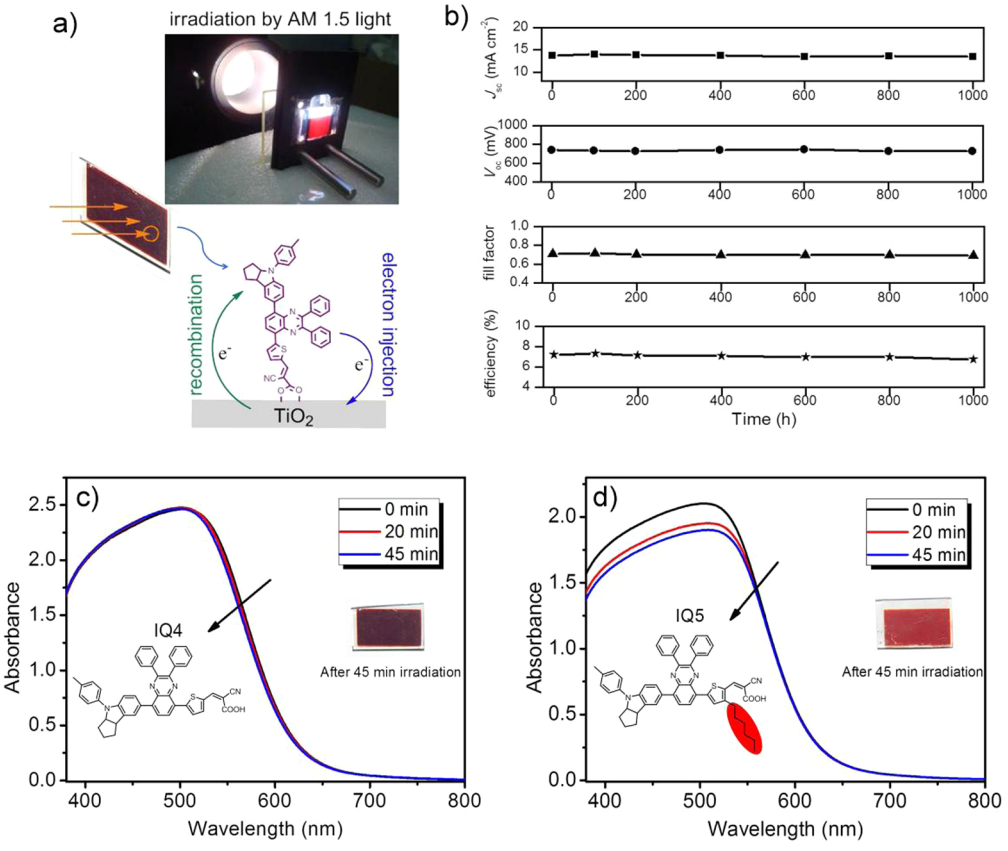

Figure 7. (a) Dye photostability measurement on the TiO_2 film and schematic diagram of the aging process upon light irradiation on a dye-loaded TiO_2 film. (b) Evolution of the photovoltaic parameters for **IQ_4**-based DSSC under 1 sun soaking at 60 °C over a period of 1000 h. Absorption spectra of (c) **IQ_4** and (d) **IQ_5** adsorbed on nanocrystalline TiO_2 films before (black line) and after light irradiation for 20 min (red line) and 45 min (blue line).

during a 1000 h aging test under 1 sun at 60 °C. These results enable the high possibility of practical application of **IQ$_4$**.[82]

CONCLUSIONS

To date, only a few pure metal-free organic sensitizers based on an iodine electrolyte are capable of achieving 9% in photovoltaic efficiency. For overcoming the photovoltaic bottleneck, we have successfully incorporated an electron-withdrawing unit of 2,3-diphenylquinoxaline as the additional acceptor to construct a novel D−A−π−A-featured dye **IQ$_4$**. Investigated theoretically by DFT and TDDFT, the incorporated auxiliary quinoxaline unit with low band gap can efficiently optimize the energy levels and broaden the absorption band. Notably, **IQ$_4$**-sensitized DSSCs successfully achieve promising power conversion efficiency up to 9.24 ± 0.05%, making an ideal balance in both the preferable photocurrent and photovoltage. Because of steric restriction of two phenyl groups, 2,3-diphenylquinoxaline is demonstrated as an efficient building block for achieving high V_{oc}, endowing a strong capability of restraining intermolecular aggregation with ideal morphology for reducing charge recombination. We expect that the promising unit of 2,3-diphenylquinoxaline will motivate the development of high-efficiency coadsorbent-free organic sensitizers, instead of the common, stability-deleterious alkyl chain substituted on the thienyl π bridge.

EXPERIMENTAL SECTION

Characterization. ^{1}H and ^{13}C NMR spectra were recorded on a Bruker AVANCE III-400 MHz (100 MHz for ^{13}C NMR) instrument with tetramethylsilane as the internal standard. High-resolution mass spectrometry (HRMS) was performed using a Waters LCT Premier XE spectrometer. The absorption spectra of sensitizer dyes in solution and adsorbed on TiO_2 films were measured with a Varian Cary 500 spectrophotometer. CV was determined with a Versastat II electrochemical workstation (Princeton Applied Research) using a three-electrode cell with a platinum working electrode, a platinum wire auxiliary electrode, and a saturated calomel reference electrode in a saturated KCl solution, and 0.1 M tetrabutylammonium hexafluorophosphate was used as the supporting electrolyte in CH_2Cl_2. Ferrocene was added to each sample solution at the end of the experiments, and the ferrocenium/ferrocene (Fc/Fc^+) redox couple was used as an internal potential reference.

Synthesis. The synthetic routes to the two sensitizers are depicted in Scheme S1 in the SI. Both **IQ$_4$** and **IQ$_5$** were synthesized from the starting material of 5,8-dibromo-2,3-diphenylquinoxaline. Via common Suzuki coupling and Vilsmeier−Haack and Knoevenagel condensation reactions, the targeted sensitizers were obtained in moderate yield. The sensitizers and important intermediates were well-characterized by ^{1}H and ^{13}C NMR and HRMS.

Synthesis of IQ$_4$. A mixture of aldehyde **1b** (250 mg, 0.39 mmol) and cyanoacetic acid (85 mg, 1.00 mmol) in acetonitrile (20 mL) was refluxed in the presence of piperidine (1 mL) for 7 h under argon. After cooling, the mixture was diluted with CH_2Cl_2, washed with water and brine, dried over Na_2SO_4, and evaporated under reduced pressure. The crude product was purified by column chromatography with 1% AcOH in CH_2Cl_2 on silica gel to yield the product as a purple powder (160 mg, 0.23 mmol, yield 58%). ^{1}H NMR (400 MHz, DMSO-d_6, δ): 12.12−13.81 (b, 1H, −COOH), 8.31−8.58 (m, 2H, Ph−H and =C*H*−), 8.07 (s, 1H, thienyl−H), 7.98 (s, 1H, thienyl−H), 7.74−7.88 (m, 3H, Ph−H), 7.70 (s, 1H, Ph−H), 7.56 (d, J = 6.4 Hz, 2H, Ph−H), 7.27−7.51 (m, 7H, Ph−H), 7.09−7.26 (m, 4H, Ph−H), 6.93 (d, J = 7.2 Hz, 1H, Ph−H), 4.77−4.96 (m, 1H, NC*H*CH−), 3.73−3.99 (m, 1H, NCHC*H*−), 2.29 (s, 3H, Ph−CH_3), 2.01−2.18 (m, 1H, indoline−H), 1.70−1.88 (m, 3H, indoline−H), 1.58−1.70 (m, 1H, indoline−H), 1.36−1.51 (m, 1H, indoline−H). ^{13}C NMR (100 MHz, DMSO-d_6, δ): 163.44, 151.67, 151.36, 148.32, 146.25, 139.26, 138.60, 138.44, 138.27, 137.22, 137.04, 132.09, 130.64, 130.08, 129.94, 129.50, 128.67, 128.59, 128.40, 127.83, 126.22, 119.89, 116.10, 98.20, 69.00, 53.96, 48.95, 45.46, 19.94. HRMS (ESI, m/z, $[M + H]^+$). Calcd for $C_{46}H_{35}N_4O_2S$: 707.2481. Found: 707.2480.

Synthesis of IQ$_5$. A mixture of aldehyde **2c** (280 mg, 0.39 mmol) and cyanoacetic acid (85 mg, 1 mmol) in acetonitrile (20 mL) was refluxed in the presence of piperidine (1 mL) for 7 h under argon. After cooling, the mixture was diluted with CH_2Cl_2, washed with water and brine, dried over Na_2SO_4, and evaporated under reduced pressure. The crude product was purified by column chromatography with 1% AcOH in CH_2Cl_2 on silica gel to yield the product as a purple powder (200 mg, 0.25 mmol, yield 64%). ^{1}H NMR (400 MHz, DMSO-d_6, δ): 13.0−14.6 (b, 1H, −COOH), 8.37 (d, J = 8.0 Hz, 1H, alkene−H), 8.31 (s, 1H, Ph−H), 7.94 (s, 1H, Ph−H), 7.75−7.88 (m, 3H, thienyl−H and Ph−H), 7.67 (s, 1H, Ph−H), 7.57 (d, J = 6.8 Hz, 2H, Ph−H), 7.28−7.50 (m, 7H), 7.23 (d, J = 8.4 Hz, 2H, Ph−H), 7.19 (d, J = 8.8 Hz, 2H, Ph−H), 6.94 (d, J = 6.8 Hz, 1H, Ph−H), 4.82−4.94 (m, 1H, NC*H*CH−), 3.80−3.91 (m, 1H, NCHC*H*−), 2.71−2.81 (t, J = 7.6 Hz, 2H, hexyl−$CH_2C_5H_{11}$), 2.29 (s, 3H, Ph−CH_3), 2.03−2.15 (m, 1H, indoline−H), 1.86−1.96 (m, 1H, indoline−H), 1.71−1.86 (m, 2H, indoline−H), 1.55−1.71 (m, 3H, indoline−H and hexyl−$CH_2CH_2C_3H_6CH_3$), 1.39−1.50 (m, 1H, indoline−H), 1.22−1.37 (m, 6H, hexyl−$C_2H_4C_3H_6CH_3$), 0.86 (t, J = 7.2 Hz, 3H, hexyl−CH_3). ^{13}C NMR (100 MHz, DMSO-d_6, δ): 164.17, 151.03, 151.00, 147.21, 140.08, 139.58, 138.61, 137.69, 137.34, 136.36, 134.19, 132.38, 130.64, 130.29, 129.89, 129.73, 128.96, 128.76, 128.53, 128.41, 128.02, 127.82, 127.52, 126.97, 119.47, 117.24, 106.44, 68.24, 44.63, 34.74, 33.16, 30.93, 30.54, 28.42, 28.13, 24.03, 22.02, 20.37, 13.90. HRMS (ESI, m/z, $[M + H]^+$). Calcd for $C_{52}H_{47}N_4O_2S$: 791.3420. Found: 791.3414.

DSSC Fabrication and Photovoltaic Performance Measurements. A double-layer TiO_2 photoelectrode of 17 μm thickness, composed of a 12-μm-thick nanoporous layer and a 5-mm-thick scattering layer (area: 0.25 cm^2), was prepared by screen printing on a conducting glass substrate. A dye solution of **IQ$_4$** and **IQ$_5$** with a 3 × 10^{-4} M concentration in 3:7 (v/v) $CHCl_3$/EtOH was used to uptake the dye onto the TiO_2 film. Deoxycholic acid (DCA, 20 mM) was added into the **IQ$_4$** solution as a coadsorbent to investigate the aggregation effect. The TiO_2 films were immersed in the dye solution and then kept at 25 °C for 40 h. Photovoltaic measurements were performed in a sandwich-type solar cell in conjunction with an electrolyte consisting of a solution of 0.6 M dimethylpropylimidazolium iodide, 0.05 M I_2, 0.1 M LiI, and 0.5−1.0 M TBP in acetonitrile. The dye-deposited TiO_2 film and a platinum-coated conducting glass were separated by a Surlyn spacer (40 μm thick) and sealed by heating the polymer frame. The photocurrent density−voltage (I−V) of sealed solar cells was measured with a black metal mask of 0.25 cm^2, illuminating the cell through the conducting glass from the anode side with a solar simulator (WXS-155S-10) at AM 1.5 illumination (light intensities: 100 mW cm^{-2}). Monochromatic IPCE was measured with monochromatic incident light of 1 × 10^{16} photons cm^{-2} under 100 mW cm^{-2} in director current mode measurements, which were made on a CEP-2000 system (Bunkoh-Keiki Co. Ltd.).

EIS Measurements. The EIS spectra were measured with an impedance analyzer (Solartron Analytical, 1255B) connected with a potentiostat (Solartron Analytical, 1287) in the dark using a solar simulator (WXS-155S-10: Wacom Denso Co. Japan). EIS spectra were recorded over a frequency range of 10^{-2}−10^6 Hz at 25 °C. The applied bias voltage was set at a V_{oc} of the DSSCs and a potential perturbation of 10 mV was applied to the testing cell, with a frequency range of 100 mHz to 100 kHz. The EIS spectra were characterized using *Z-View* software (Solartron Analytical).

ASSOCIATED CONTENT

Supporting Information

Experimental section, frontier molecular orbitals of **IQ$_4$** calculated at the B3LYP/6-31G level of theory, and ^{1}H and ^{13}C NMR and HRMS of **IQ$_4$** and **IQ$_5$**. This material is available free of charge via the Internet at http://pubs.acs.org.

AUTHOR INFORMATION

Corresponding Author

*Fax: +81-29-859-2304 (L.H.), (+86) 21-6425-2758 (W.Z.). E-mail: Han.Liyuan@nims.go.jp (L.H.), whzhu@ecust.edu.cn (W.Z.).

Notes

The authors declare no competing financial interest.

ACKNOWLEDGMENTS

This work was financially supported by NSFC/China, National 973 Program (2013CB733700), the Oriental Scholarship, SRFDP 20120074110002, the Fundamental Research Funds for the Central Universities (WK1013002), STCSM (10dz2220500), Core Research for Evolutional Science and Technology (CREST) of the Japan Science and Technology Agency, and the Open Funding Project of State Key Laboratory of Luminescent Materials and Devices (SCUT).

REFERENCES

(1) O'Regan, B.; Grätzel, M. *Nature* **1991**, *353*, 737−740.
(2) Ooyama, Y.; Harima, Y. *ChemPhysChem* **2012**, *13*, 4032−4080.
(3) Roncali, J. *Adv. Energy Mater.* **2011**, *1*, 147−160.
(4) Yella, A.; Lee, H. W.; Tsao, H. N.; Yi, C. Y.; Chandiran, A. K.; Nazeeruddin, M. K.; Diau, E. W. G.; Yeh, C. Y.; Zakeeruddin, S. M.; Grätzel, M. *Science* **2011**, *334*, 629−634.
(5) Mao, J. Y.; He, N. N.; Ning, Z. J.; Zhang, Q.; Guo, F. L.; Chen, L.; Wu, W. J.; Hua, J. L.; Tian, H. *Angew. Chem., Int. Ed.* **2012**, *51*, 9873−9876.
(6) Sepehrifard, A.; Kamino, B. A.; Bender, T. P.; Morin, S. *ACS Appl. Mater. Interfaces* **2012**, *4*, 6211−6215.
(7) Li, C.; Wonneberger, H. *Adv. Mater.* **2012**, *24*, 613−636.
(8) Numata, Y.; Singh, S. P.; Islam, A.; Iwamura, M.; Imai, A.; Nozaki, K.; Han, L. Y. *Adv. Funct. Mater.* **2012**, *23*, 1817−1823.
(9) Mishra, A.; Fischer, M. K. R.; Baüerle, P. *Angew. Chem., Int. Ed.* **2009**, *48*, 2474−2499.
(10) Hagfeldt, A.; Boschloo, G.; Sun, L. C.; Kloo, L.; Pettersson, H. *Chem. Rev.* **2010**, *110*, 6595−6663.
(11) Yen, Y. S.; Chou, H. H.; Chen, Y. C.; Hsu, C. Y.; Lin, J. T. *J. Mater. Chem.* **2012**, *22*, 8734−8747.
(12) Wu, Y. Z.; Zhu, W. H. *Chem. Soc. Rev.* **2013**, *42*, 2039−2058.
(13) Zeng, W. D.; Cao, Y. M.; Bai, Y.; Wang, Y. H.; Shi, Y. S.; Zhang, M.; Wang, F. F.; Pan, C. Y.; Wang, P. *Chem. Mater.* **2010**, *22*, 1915−1925.
(14) Zhang, G. L.; Bala, H.; Cheng, Y. M.; Shi, D.; Lv, X. J.; Yu, Q. J.; Wang, P. *Chem. Commun.* **2009**, 2198−2200.
(15) Wu, Y. Z.; Marszalek, M.; Zakeeruddin, S. M.; Zhang, Q.; Tian, H.; Grätzel, M.; Zhu, W. H. *Energy Environ. Sci.* **2012**, *5*, 8261−8272.
(16) Ito, S.; Miura, H.; Uchida, S.; Takata, M.; Sumioka, K.; Liska, P.; Comte, P.; Pechy, P.; Grätzel, M. *Chem. Commun.* **2008**, 5194−5196.
(17) Kim, B. G.; Zhen, C. G.; Jeong, E. J.; Kieffer, J.; Kim, J. *Adv. Funct. Mater.* **2012**, *22*, 1606−1612.
(18) Miyashita, M.; Sunahara, K.; Nishikawa, T.; Uemura, Y.; Koumura, N.; Hara, K.; Mori, A.; Abe, T.; Suzuki, E.; Mori, S. *J. Am. Chem. Soc.* **2008**, *130*, 17874−17881.
(19) Gao, F.; Wang, Y.; Shi, D.; Zhang, J.; Wang, M.; Jing, X.; Humphry-Baker, R.; Wang, P.; Zakeeruddin, S. M.; Grätzel, M. *J. Am. Chem. Soc.* **2008**, *130*, 10720−10728.
(20) Liang, M.; Chen, J. *Chem. Soc. Rev.* **2013**, *42*, 3453−3488.
(21) Labat, F.; Bahers, T.; Ciofini, I.; Adamo, C. *Acc. Chem. Res.* **2012**, *45*, 1268−1277.
(22) Stergiopoulos, T.; Falaras, P. *Adv. Energy Mater.* **2012**, *2*, 612−627.
(23) Clifford, J. N.; Martinez-Ferrero, E.; Viterisi, A.; Palomares, E. *Chem. Soc. Rev.* **2011**, *40*, 1635−1646.
(24) Ning, Z. J.; Fu, Y.; Tian, H. *Energy Environ. Sci.* **2010**, *3*, 1170−1181.
(25) Anderson, A. Y.; Barnes, P. R. F.; Durrant, J. R.; O'Regan, B. C. *J. Phys. Chem. C* **2011**, *115*, 2439−2447.
(26) Takacs, C. J.; Sun, Y. M.; Welch, G. C.; Perez, L. A.; Liu, X. F.; Wen, W.; Bazan, G. C.; Heeger, A. J. *J. Am. Chem. Soc.* **2012**, *134*, 16597−16606.
(27) Numata, Y.; Islam, A.; Chen, H.; Han, L. Y. *Energy Environ. Sci.* **2012**, *5*, 8548−8552.
(28) Ren, X. M.; Jiang, S. H.; Cha, M. Y.; Zhou, G.; Wang, Z. S. *Chem. Mater.* **2012**, *24*, 3493−3499.
(29) Chen, T.; Hu, W. H.; Song, J. L.; Guai, G. H.; Li, C. M. *Adv. Funct. Mater.* **2012**, *22*, 5245−5250.
(30) Lan, C.; Wu, H.; Pan, T.; Chang, C.; Chao, W.; Chen, C.; Wang, C.; Lin, C.; Diau, E. W. *Energy Environ. Sci.* **2012**, *5*, 6460−6464.
(31) Koumura, N.; Wang, Z. S.; Mori, S.; Miyashita, M.; Suzuki, E.; Hara, K. *J. Am. Chem. Soc.* **2006**, *128*, 14256−14257.
(32) Wang, Z. S.; Koumura, N.; Cui, Y.; Takahashi, M.; Sekiguchi, H.; Mori, A.; Kubo, T.; Furube, A.; Hara, K. *Chem. Mater.* **2008**, *20*, 3993−4003.
(33) Zhang, G.; Bala, H.; Cheng, Y.; Shi, D.; Lv, X.; Yu, Q.; Wang, P. *Chem. Commun.* **2009**, 2198−2200.
(34) Li, W. Q.; Wu, Y. Z.; Li, X.; Xie, Y. S.; Zhu, W. H. *Energy Environ. Sci.* **2011**, *4*, 1830−1837.
(35) Liu, B.; Liu, Q. B.; You, D.; Li, X. Y.; Naruta, Y.; Zhu, W. H. *J. Mater. Chem.* **2012**, *22*, 13348−13356.
(36) Ito, S.; Miura, H.; Uchida, S.; Takata, M.; Sumioka, K.; Liska, P.; Comte, P.; Pechy, P.; Grätzel, M. *Chem. Commun.* **2008**, 5194−5196.
(37) Ning, Z. J.; Zhang, Q.; Wu, W. J.; Pei, H.; Liu, B.; Tian, H. *J. Org. Chem.* **2008**, *73*, 3791−3797.
(38) Jørgensen, M.; Norrman, K.; Gevorgyan, S. A.; Tromholt, T.; Andreasen, B.; Krebs, F. C. *Adv. Mater.* **2012**, *24*, 580−612.
(39) Manceau, M.; Chambon, S.; Rivaton, A.; Gardette, J.; Guillerez, S.; Lemaître, N. *Sol. Energy Mater. Sol. Cells* **2010**, *94*, 1572−1577.
(40) Velusamy, M.; Thomas, K. R. J.; Lin, J. T.; Hsu, Y. C.; Ho, K. C. *Org. Lett.* **2005**, *7*, 1899−1902.
(41) Kim, J.; Choi, H.; Lee, J.; Kang, M.; Song, K.; Kang, S. O.; Ko, J. *J. Mater. Chem.* **2008**, *18*, 5223−5229.
(42) Tang, Z. M.; Lei, T.; Jiang, K. J.; Song, Y. L.; Pei, J. *Chem.—Asian J.* **2010**, *5*, 1911−1917.
(43) Haid, S.; Marszalek, M.; Mishra, A.; Wielopolski, M.; Teuscher, J.; Moser, J.; Humphry-Baker, R.; Zakeeruddin, S. M.; Grätzel, M.; Bäuerle, P. *Adv. Funct. Mater.* **2012**, *22*, 1291−1302.
(44) Qu, S. Y.; Qin, C. J.; Islam, A.; Wu, Y. Z.; Zhu, W. H.; Hua, J. L.; Tian, H.; Han, L. Y. *Chem. Commun.* **2012**, *48*, 6972−6974.
(45) Feng, Q. Y.; Lu, X. F.; Zhou, G.; Wang, Z. S. *Phys. Chem. Chem. Phys.* **2012**, *14*, 7993−7999.
(46) Wang, Z. S.; Cui, Y.; Hara, K.; Dan-oh, Y.; Kasada, C.; Shinpo, A. *Adv. Mater.* **2007**, *19*, 1138−1141.
(47) Chen, B. S.; Chen, D. Y.; Chen, C. L.; Hsu, C. W.; Hsu, H. C.; Wu, K. L.; Liu, S. H.; Chou, P. T.; Chi, Y. *J. Mater. Chem.* **2011**, *21*, 1937−1945.
(48) Zhu, W. H.; Wu, Y. Z.; Wang, Z. S.; Li, W. Q.; Li, X.; Chen, J.; Wang, Z. S.; Tian, H. *Adv. Funct. Mater.* **2011**, *21*, 756−763.
(49) Wu, Y. Z.; Zhang, X.; Li, W. Q.; Wang, Z. S.; Tian, H.; Zhu, W. H. *Adv. Energy Mater.* **2012**, *2*, 149−156.
(50) Li, W. Q.; Wu, Y. Z.; Zhang, Q.; Tian, H.; Zhu, W. H. *ACS Appl. Mater. Interfaces* **2012**, *4*, 1822−1830.
(51) Cui, Y.; Wu, Y. Z.; Lu, X. F.; Zhang, X.; Zhou, G.; Miapeh, F. B.; Zhu, W. H.; Wang, Z. S. *Chem. Mater.* **2011**, *23*, 4394−4401.
(52) Ding, W. L.; Wang, D. M.; Geng, Z. Y.; Zhao, X. L.; Xu, W. B. *Dyes Pigm.* **2013**, *98*, 125−135.
(53) Chang, D. W.; Lee, H. J.; Kim, J. H.; Park, S. Y.; Park, S.; Dai, L.; Baek, J. *Org. Lett.* **2011**, *13*, 3880−3883.
(54) Pei, K.; Wu, Y. Z.; Wu, W. J.; Zhang, Q.; Chen, B. Q.; Tian, H.; Zhu, W. H. *Chem.—Eur. J.* **2012**, *18*, 8190−8200.
(55) Shi, J.; Chen, J. N.; Chai, Z. F.; Wang, H.; Tang, R.; Fan, K.; Wu, M.; Han, H. W.; Qin, J. G.; Peng, T.; Li, Q. Q.; Li, Z. *J. Mater. Chem.* **2012**, *22*, 18830−18838.
(56) Lu, X. F.; Feng, Q. Y.; Lan, T.; Zhou, G.; Wang, Z. S. *Chem. Mater.* **2012**, *24*, 3179−3187.

(57) Li, S. R.; Lee, C. P.; Kuo, H. T.; Ho, K. C.; Sun, S. S. *Chem.—Eur. J.* **2012**, *18*, 12085−12095.
(58) Liu, B.; Zhu, W. H.; Zhang, Q.; Wu, W. J.; Xu, M.; Ning, Z. J.; Xie, Y. S.; Tian, H. *Chem. Commun.* **2009**, 1766−1768.
(59) Ito, S.; Zakeeruddin, S. M.; Humphry-Baker, R.; Liska, P.; Charvet, R.; Comte, P.; Nazeeruddin, M. K.; Péchy, P.; Takata, M.; Miura, H.; Uchida, S.; Grätzel, M. *Adv. Mater.* **2006**, *18*, 1202−1205.
(60) Schmidt-Mende, L.; Bach, U.; Humphry-Baker, R.; Horiuchi, T.; Miura, H.; Ito, S.; Uchida, S.; Grätzel, M. *Adv. Mater.* **2005**, *17*, 813−815.
(61) Dentani, T.; Kubota, Y.; Funabiki, K.; Jin, J.; Yoshida, T.; Minoura, H.; Miura, H.; Matsui, M. *New J. Chem.* **2009**, *33*, 93−101.
(62) Ning, Z. J.; Zhou, Y. C.; Zhang, Q.; Ma, D. G.; Zhang, J. J.; Tian, H. *J. Photochem. Photobiol. A: Chem.* **2007**, *192*, 8−16.
(63) Hagfeldt, A.; Grätzel, M. *Chem. Rev.* **1995**, *95*, 49−68.
(64) Lynch J, B.; Fast, P. L.; Harris, M.; Truhlar, D. G. *J. Phys. Chem. A* **2000**, *104*, 4811−4815.
(65) Frisch, M. J.; Trucks, G. W.; Schlegel, H. B.; Scuseria, G. E.; Robb, M. A.; Cheeseman, J. R.; Scalmani, G.; Barone, V.; Mennucci, B.; Petersson, G. A.; Nakatsuji, H.; Caricato, M.; Li, X.; Hratchian, H. P.; Izmaylov, A. F.; Bloino, J.; Zheng, G.; Sonnenberg, J. L.; Hada, M.; Ehara, M.; Toyota, K.; Fukuda, R.; Hasegawa, J.; Ishida, M.; Nakajima, T.; Honda, Y.; Kitao, O.; Nakai, H.; Vreven, T.; Montgomery, J. A., Jr.; Peralta, J. J. E.; Ogliaro, F.; Bearpark, M.; Heyd, J. J.; Brothers, E.; Kudin, K. N.; Staroverov, V. N.; Kobayashi, R.; Normand, J.; Raghavachari, K.; Rendell, A.; Burant, J. C.; Iyengar, S. S.; Tomasi, J.; Cossi, M.; Rega, N.; Millam, J. M.; Klene, M.; Knox, J. E.; Cross, J. B.; Bakken, V.; Adamo, C.; Jaramillo, J.; Gomperts, R.; Stratmann, R. E.; Yazyev, O.; Austin, A. J.; Cammi, R.; Pomelli, C.; Ochterski, J. W.; Martin, R. L.; Morokuma, K.; Zakrzewski, V. G.; Voth, G. A.; Salvador, P.; Dannenberg, J. J.; Dapprich, S.; Daniels, A. D.; Farkas, O.; Foresman, J. B.; Ortiz, J. V.; Cioslowski, J.; Fox, D. J. *Gaussian 09*, revision A.02; Gaussian, Inc.: Wallingford, CT, 2009.
(66) Yin, X.; Zhao, H.; Chen, L. P.; Tan, W. W.; Zhang, J. B.; Weng, Y. X.; Shuai, Z. G.; Xiao, X. R.; Zhou, X.; Li, X. P.; Lin, Y. *Surf. Interface Anal.* **2007**, *37*, 809−816.
(67) Schlichthorl, G.; Huang, S. Y.; Sprague, J.; Frank, A. J. *J. Phys. Chem. B* **1997**, *101*, 8141−8155.
(68) Mikoshiba, S.; Murai, S.; Sumino, H.; Hayase, S. *Chem. Lett.* **2002**, 1156−1157.
(69) Wu, K. L.; Li, C. H.; Chi, Y.; Clifford, J. N.; Cabau, L.; Palomares, E.; Cheng, Y. M.; Pan, H. A.; Chou, P. T. *J. Am. Chem. Soc.* **2012**, *134*, 7488−7496.
(70) Chang, Y. J.; Chow, T. J. *J. Mater. Chem.* **2011**, *21*, 9523−9531.
(71) Adachi, M.; Sakamoto, M.; Jiu, J.; Ogata, Y.; Isoda, S. *J. Phys. Chem. B* **2006**, *110*, 13872−13880.
(72) Pijpers, J. J. H.; Ulbricht, R.; Derossi, S.; Reek, J. N. H.; Bonn, M. *J. Phys. Chem. C* **2011**, *115*, 2578−2584.
(73) Bisquert, J.; Mora-Seró, I. *J. Phys. Chem. Lett.* **2010**, *1*, 450−456.
(74) Wang, Q.; Moser, J. E.; Grätzel, M. *J. Phys. Chem. B* **2005**, *109*, 14945−14953.
(75) Kern, R.; Sastrawan, R.; Ferber, J.; Stangl, R.; Luther, J. *Electrochim. Acta* **2002**, *47*, 4213−4225.
(76) Bisquert, J. *J. Phys. Chem. B* **2002**, *106*, 325−333.
(77) Van de Lagemaat, J.; Park, N. G.; Frank, A. J. *J. Phys. Chem. B* **2000**, *104*, 2044−2052.
(78) Bisquert, J.; Fabregat-Santiago, F.; Mora-Seró, I.; Garcia-Belmonte, G.; Giménez, S. *J. Phys. Chem. C* **2009**, *113*, 17278−17290.
(79) Fabregat-Santiago, F.; Garcia-Belmonte, G.; Mora-Seró, I.; Bisquert, J. *Phys. Chem. Chem. Phys.* **2011**, *13*, 9083−9118.
(80) Barea, E. M.; Gónzalez-Pedro, V.; Ripollés-Sanchis, T.; Wu, H.; Li, L.; Yeh, C.; Diau, E.; Bisquert, J. *J. Phys. Chem. C* **2011**, *115*, 10898−10902.
(81) Katoh, R.; Furube, A.; Mori, S.; Miyashita, M.; Sunahara, K.; Koumura, N.; Hara, K. *Energy Environ. Sci.* **2009**, *2*, 542−546.
(82) Jung, K. H.; Bae, J. Y.; Yun, H.-G.; Kang, M. G; Bae, B. S. *ACS Appl. Mater. Interfaces* **2011**, *3*, 293−298.